Stimulated Raman scattering of an ultrashort XUV radiation pulse by a hydrogen atom

Mihai Dondera* and Viorica Florescu†
Department of Physics and Centre for Advanced Quantum Physics, University of Bucharest, MG-11, Bucharest-Măgurele, 077125, Romania

Henri Bachau‡
Centre des Lasers Intenses et Applications, Université de Bordeaux-CNRS-CEA, 33405 Talence Cedex, France
(Received 19 October 2016; published 22 February 2017)

We consider the hydrogen atom H($1s$) exposed to an ultrashort laser pulse with a central frequency ω_0 ranging from several hundreds of eV to 1.5 keV ($\approx$55 a.u.) and a peak intensity of 3.51×10^{16} W/cm^2. We study the excitation of the atom by stimulated Raman scattering, a process involving pairs of frequencies (ω_1,ω_2). These frequencies are non-negligible components of the pulse Fourier transform and they satisfy the condition $E_g + \hbar\omega_1 = E_b + \hbar\omega_2$, E_g and $E_b \equiv E_n$ being the ground-state and the excited-state energy, respectively. The numerical results obtained by integrating the time-dependent Schrödinger equation (TDSE) are compared with calculations in lowest order perturbation theory (LOPT). In LOPT we consider, in the second order of PT, the contribution of the term $\mathbf{A}\cdot\mathbf{P}$ in the dipole approximation and, in first order of PT, the expression of $\mathbf{A}^2$ taken for first-order retardation effects. ($\mathbf{A}$ denotes the vector potential of the field and $\mathbf{P}$ is the momentum operator.) We focus on the Raman excitation of bound states with principal quantum numbers n up to $n = 13$. The evaluation in perturbation theory of the $\mathbf{A}\cdot\mathbf{P}$ contribution to $1s$-ns and $1s$-nd transition probabilities uses analytic expressions of the corresponding Kramers–Heisenberg matrix elements. At fixed pulse duration $\tau = 6\pi$ a.u. ($\approx$0.48 fs), we find that the retardation effects play an important role at high frequencies: they progressively diminish as the frequency decreases until the contribution of $\mathbf{A}\cdot\mathbf{P}$ dominates over the $\mathbf{A}^2$ contribution for ω_0 values of a few a.u. We also study the dependence of the Raman process on the pulse duration for several values of ω_0. In the case $\omega_0 = 13$ a.u. ($\approx$354 eV) where dipole and nondipole contributions are of the same order of magnitude, we present the Raman excitation probability as a function of the pulse duration for excited ns, np, and nd states.

DOI: 10.1103/PhysRevA.95.023417

I. INTRODUCTION

The construction of fourth-generation free-electron laser (FEL) sources opens the way to the exploration of new regimes in atomic and electronic processes, with major applications in physics, chemistry, and biology. FELs can produce femtosecond (fs) pulses at short wavelengths and high intensities [1–3] and it is now possible to investigate nonlinear processes in XUV and x-ray regimes [4]. These last years, we have investigated stimulated Compton scattering (SCS) [5,6], which is a two-color process leading to the ionization of hydrogen atoms. It involves two photons of frequencies ω_1 and ω_2, one absorbed, the other emitted. The frequencies satisfy the condition

$$E_g + \hbar\omega_1 = E_c + \hbar\omega_2, \tag{1}$$

where E_g and E_c are the ground-state and final-continuum-state energies, respectively. Here it is worth noticing that considerable progress has been realized in the production of high-intensity two-color x rays at FELs (see Ref. [7] and other references therein), opening the pathway to investigate nonlinear processes with two colors, like SCS. The main outcome of our previous studies is that nondipole effects play a crucial role in SCS, and this for photon energies ranging from several hundreds of eV to keV [8].

In parallel with the technological progress evoked above around FELs, a considerable activity has been devoted to shorten the FEL pulse duration, from the fs to sub-fs domain and below, see Refs. [9–11] for recent works and Refs. [12,13] for reviews. Recent calculations of stimulated Raman transitions at frequencies of 30–40 eV [14] have explored the case of the sodium atom, and it has been shown that, at pulses durations of few fs (1, 3, 5 fs), Raman redistribution can overwhelm photoionization. The terminology of SRS has been given in reference to a phenomenon discovered immediately after the laser was invented [15,16].

In the present paper, following a previous letter [17], we study stimulated Raman scattering (SRS) in hydrogen by an ultrashort pulse. The pulse considered, whose duration is such that the laser bandwidth $\Delta\omega$ is of the order of (or larger than) the Bohr frequency $\omega_{bg} = (E_b - E_g)/\hbar$ (E_b being the energy of an excited bound state), provides an infinite number of pairs of frequencies ω_1 and ω_2 satisfying the condition $\omega_1 - \omega_2 = \omega_{bg}$, thus making possible SRS through the absorption of a quanta $\hbar\omega_1$ and the *stimulated* emission of another quanta $\hbar\omega_2$, accompanied by the atomic transition $g \to b$. In Ref. [17] only the case $\omega_0 = 55$ a.u. was considered and the results were obtained by numerical integration of TDSE. In a few cases we compared with perturbation theory (PT) results without giving details about the equations used. In the present paper we investigate thoroughly SRS in a domain of frequencies ranging from the XUV to soft x rays. At the peak intensity of $I_0 \equiv 3.51 \times 10^{16}$ W/cm^2 used here and for the photon energy range considered (about 100 to 1500 eV), the theory of tunneling is not valid [the photon energy is much larger than the ionization potential of H($1s$) [18]] and the concept of the multiphoton

*don@barutu.fizica.unibuc.ro
†flor@barutu.fizica.unibuc.ro
‡henri.bachau@u-bordeaux.fr

process applies. In this context the validity of the perturbation theory and of the dipole approximation remains to be checked, in particular for photon energies of a few hundred eV. We focus here on these two points.

The relative importance of the nondipole effects, through the contribution of the A^2 term and which has been already noticed in the case of SCS [5], is found also in the present study with the same explanation: the partial cancellation of the second-order contributions related to $\mathbf{A}\cdot\mathbf{P}$ in the high-frequency regime. This raises the question of determining the frequency range where nondipole effects dominate SRS.

The calculations are done in the semiclassical theory: the electromagnetic field is described classically while the quantum mechanics is used to treat the electronic structure of the atom. The electromagnetic field is taken as a pulsed plane wave with pulse durations ranging from 1 fs to 100 as. For the photon energies considered, which are well above the ionization potential, the direct excitation of the hydrogen atom by one-photon absorption is negligible, the bound-state excitation is due to nonlinear processes involving the absorption and emission of photons, like SRS.

We start Sec. II by reproducing, for further reference, the expression of the Kramers–Heisenberg–Waller (KHW) matrix element, given in Eq. (3). Then we present in Secs. II B and II C, respectively, the electromagnetic pulse and the *approximate* Hamiltonian operator used in the TDSE calculations, following the method presented in our previous publications [19,20]. We continue Sec. II by giving details on our use of time-dependent perturbation theory. We show that perturbation theory (PT) is an efficient tool for the study of SRS under our conditions of laser wavelength and intensity, both for the interpretation of TDSE results and as a "low cost" procedure to describe the studied process.

Equations (19) and (20) represent the main results of Sec. II. They show, in the case of a pulse, how the KHW matrix element, modulated by a function characterizing the pulse, determines the SRS amplitude. The numerical results in Sec. III are based on the previously mentioned equations in which the approximate form (8) is used for the KHW matrix element. It contains in the first-order of PT the retardation correction associated with the $\mathbf{A^2}$ term in the Hamiltonian and the second-order contribution of $\mathbf{A}\cdot\mathbf{P}$ in dipole approximation. An approximate formula for the transition amplitude, related to the KHW matrix element and pulse properties, is presented in Eq. (26). All the probabilities calculated within this LOPT treatment are proportional to I^2. The graphs in Sec. III illustrate the dependence of the (total and partial) Raman excitation probabilities on the central frequency and pulse duration.

II. THEORY AND METHODS

For further reference we write the exact expression of the nonrelativistic Hamiltonian for the electron in a central atomic field $V(r)$, in interaction with the electromagnetic field described in the Coulomb gauge by the potential vector $\mathbf{A}$,

$$\mathcal{H}=\frac{1}{2m_e}\mathbf{P}^2+V(r)-\frac{e}{m_e}\mathbf{A}\cdot\mathbf{P}+\frac{e^2}{2m_e}\mathbf{A}^2,\quad \boldsymbol{\nabla}\cdot\mathbf{A}=0. \tag{2}$$

In the semiclassical formalism adopted here, $\mathbf{A}$ is a function of the space coordinate $\mathbf{r}$ and time.

A. Kramers–Heisenberg–Waller matrix element for bound-bound transition

We first write the expression of the Kramers–Heisenberg–Waller matrix element between two atomic states $|g\rangle$ and $|b\rangle$ of a one-electron atom. It is convenient for what follows to mention directly the particular case in which the absorbed photon and the emitted photon of frequency ω and ω', respectively, have the same direction of propagation $\mathbf{n}$ and the same linear polarization, taken as the z axis of the reference system,

$$\begin{aligned}\mathcal{M}_{bg}^{\mathrm{KHW}}(\omega,\omega')&=\frac{1}{m_e}\langle b|e^{-i\frac{\omega'}{c}\mathbf{n}\cdot\mathbf{r}}P_zG^{(+)}(E_g+\hbar\omega)e^{i\frac{\omega}{c}\mathbf{n}\cdot\mathbf{r}}P_z|g\rangle\\&+\frac{1}{m_e}\langle b|e^{i\frac{\omega}{c}\mathbf{n}\cdot\mathbf{r}}P_zG^{(+)}(E_g-\hbar\omega')e^{-i\frac{\omega'}{c}\mathbf{n}\cdot\mathbf{r}}P_z|g\rangle\\&+\langle b|e^{i\frac{\omega_{bg}}{c}\mathbf{n}\cdot\mathbf{r}}|g\rangle.\end{aligned} \tag{3}$$

The two frequencies ω and ω' are connected by $E_g+\hbar\omega=E_b+\hbar\omega'$. We have attached the label "KHW" in reference to the names of Kramers and Heisenberg [21] who, by using the principle of correspondence, introduced the formula in a study of elastic radiation scattering on an atom, and Waller [22] to whom the introduction of retardation effects is due. The first two terms, representing the second-order PT contribution of the term linear in the potential vector in the Hamiltonian (2), involve the Green (resolvent) operator $G^{(+)}(W)=G(W+i\varepsilon)=(W+i\varepsilon-H_a)^{-1}$ and the last term is the first-order contribution of the $\mathbf{A}^2$ term in the Hamiltonian.

In dipole approximation the last term vanishes and the matrix element reads

$$\begin{aligned}\mathcal{M}_{bg}^{KH}(\omega,\omega')&=\frac{1}{m_e}\langle b|P_zG^{(+)}(E_g+\hbar\omega)P_z|g\rangle\\&+\frac{1}{m_e}\langle b|P_zG^{(+)}(E_g-\hbar\omega')P_z|g\rangle\end{aligned} \tag{4}$$

or, in more compact form

$$\mathcal{M}_{bg}^{KH}(\omega,\omega')=\Pi_{33}^{DA}(E_g+\hbar\omega)+\Pi_{33}^{DA}(E_g-\hbar\omega'), \tag{5}$$

with

$$\Pi_{33}^{DA}(\Omega)\equiv\frac{1}{m_e}\langle b|P_zG^{(+)}(\Omega)P_z|g\rangle. \tag{6}$$

Note that now we use the upper subscript KH. Because the ground state is an s ($l=0$) state, the Kramers–Heisenberg amplitude leads to final s and d excited states.

The first retardation correction in the expansion in $1/c$ of the last term of Eq. (3),

$$i\frac{\omega_{bg}}{c}\mathbf{n}\cdot\mathbf{r}_{bg}, \tag{7}$$

with $\mathbf{r}_{bg}$ being the electron position matrix element, leads to p excited states.

In the case of the Coulomb field, the matrix element (5) can be analytically expressed in closed form, as shown in the Appendix.

The approximate expression of the SRS amplitude involved in our calculations uses the "hybrid" form of the matrix element (3), which only includes the dipole approximation for the $\mathbf{A}\cdot\mathbf{P}$ terms and the first nondipole correction originating from the term $\mathbf{A}^2$,

$$\mathcal{M}_{bg}^{(hyb)}(\omega,\omega') \equiv \mathcal{M}_{bg}^{(KH)}(\omega,\omega') + i\frac{\omega_{bg}}{c}\mathbf{n}\cdot\mathbf{r}_{bg}. \quad (8)$$

B. Electromagnetic radiation pulse

The radiation pulse, taken with linear polarization along the z axis and propagating along the direction $\mathbf{n}$ in the xy plane, is described by a vector potential oriented along the z axis with an amplitude $A = A(t')$, $t' = t - \mathbf{n}\cdot\mathbf{r}/c$. The function $A(t')$ is conveniently expressed as $A(t') = A_0 f(t')$, where A_0 is its peak value and $f(t')$ is its carrier multiplied by a slowly varying envelope. For numerical simulations, as in our precedent works, $A(t)$ is nonzero over a time interval $(-\tau/2, \tau/2)$ where τ is the total pulse duration, and is chosen to have a $\cos^2$ envelope.

The spectral properties of the pulse are characterized with the Fourier transform $\varphi(\omega)$ of the function $f(t)$:

$$\varphi(\omega) = \int f(t)e^{i\omega t}dt, \quad f(t) = \frac{1}{2\pi}\int \varphi(\omega)e^{-i\omega t}d\omega. \quad (9)$$

The function $|\varphi(\omega)|$ reaches its maximum value for $\omega = \pm\omega_0$, where ω_0 is the central frequency of the pulse. An important parameter for the process under study is the spectral width $\Delta\omega$ of the pulse, defined as the full width at half maximum (FWHM) of $|\varphi(\omega)|^2$, and given in the case of a $\cos^2$ pulse by $\Delta\omega \approx 1.44\omega_0/N$, where N is the number of carrier cycles.

It will be seen in Sec. II E that, for the SRS description in PT [see in particular Eq. (20)], the properties of the function

$$\Phi(\omega_{bg},\omega) \equiv \varphi(\omega)\varphi(\omega_{bg}-\omega) = \varphi(\omega)\varphi^*(\omega-\omega_{bg}), \quad (10)$$

where ω_{bg} is a Bohr frequency, play a decisive role. Here we note that, for a quasimonochromatic pulse (i.e., a pulse with very long duration), the function Φ takes negligible values due to the fact that the laser bandwidth $\Delta\omega$ goes to zero as the pulse duration increases to infinity.

C. Approximate semiclassical Hamiltonian

With the laser pulse introduced in the Sec. II B, the Hamiltonian operator (2) becomes

$$\mathcal{H} = \frac{1}{2m_e}\mathbf{P}^2 + V(r) - \frac{e}{m_e}A(t')P_z + \frac{e^2}{2m_e}A^2(t'), \quad \text{with } t' = t - \mathbf{n}\cdot\mathbf{r}/c, \quad (11)$$

where $V(r) = -e^2/4\pi\varepsilon_0 r$ is the atomic potential ($e<0$ is the electron charge in SI units). This expression is used as starting point in Sec. II E to build the transition amplitudes in PT. For the numerical integration of the TDSE, we adopt an approximate form of the potential vector in the Hamiltonian [5]; with the choice of x axis taken along the pulse propagation direction $\mathbf{n}$, $\mathbf{A}(\mathbf{t}')$ is given to a first approximation by

$$A(t') \approx A(t) + F(t)x/c, \quad (12)$$

where $F(t) \equiv -\dot{A}(t)$ is the electric field in dipole approximation, and we get

$$\mathcal{H} \approx H_a + \mathcal{H}_{DA}^{(1)} + \mathcal{H}_{\mathrm{RET}}^{(1)} + \mathcal{H}_{\mathrm{RET}}^{(2)}. \quad (13)$$

This approximate Hamiltonian is written as a sum of the atomic Hamiltonian $H_a \equiv \mathbf{P}^2/2m_e + V$, of the interaction term in dipole approximation (DA), $\mathcal{H}_{DA}^{(1)} \equiv -(e/m_e)A(t)P_z$, and of two other terms describing nondipole corrections: $\mathcal{H}_{\mathrm{RET}}^{(1)} \equiv -(e/m_e c)F(t)xP_z$ and $\mathcal{H}_{\mathrm{RET}}^{(2)} \equiv (e^2/m_e c)F(t)A(t)x$. We note that we neglected the terms of higher order in $1/c$—a procedure justified in the nonrelativistic theory—as in the present case. At the same time we remark that the interaction terms have a very simple structure (a time-dependent function multiplied by a time-independent electron operator), which is very convenient for numerical calculations. We also recall the different selection rules associated to the three interaction terms ($l' = l \pm 1;\ m' = m$) for $\mathcal{H}_{DA}^{(1)}$,($l' = l, l \pm 2;\ m' = m \pm 1$) for $\mathcal{H}_{\mathrm{RET}}^{(1)}$, and ($l' = l \pm 1;\ m' = m \pm 1$) for $\mathcal{H}_{\mathrm{RET}}^{(2)}$.

D. Nonperturbative approach

For the numerical integration of the TDSE corresponding to the approximate Hamiltonian (13) we have used a spectral method based on the expansion of the wave function

$$\psi(\mathbf{r},t) = \sum_{n,l,m} e^{-iE_{nl}t}c_n^{(l,m)}(t)u_{nlm}(\mathbf{r}) \quad (14)$$

in a discrete basis of the atomic Hamiltonian H_a—for details see Refs. [19,20]. The coupled differential equations satisfied by the coefficients $c_n^{(l,m)}(t)$ are integrated over the pulse duration by using a Runge–Kutta method, with initial conditions corresponding to the atom in the ground state $1s$. The populations of the excited states at the end of the pulse are simply calculated by taking the squared moduli of the coefficients in Eq. (14) at $t = \tau/2$.

E. Perturbative method

Our approach relies on the time-dependent PT applied to the Hamiltonian expressed in Eq. (11), where the terms $A^2(t')$ and $A(t')P_z$ are treated in first and second order of PT, respectively. The time integrals involved in the general expression of the transition amplitude $\mathcal{A}_{g\to b}$ can be performed by using the Fourier transform $\varphi(\omega)$ of the vector potential scaled to its peak value, $A(t)/A_0$, defined in Eq. (9). We give directly the compact result obtained:

$$\mathcal{A}_{g\to b} = \frac{1}{2\pi i\hbar}\frac{(eA_0)^2}{m_e}\int d\omega\varphi(\omega)\varphi(\omega_{bg}-\omega)\mathcal{T}_{bg}(\omega), \quad (15)$$

where the integral in ω is on the real axis and

$$\mathcal{T}_{bg}(\omega) \equiv \frac{1}{m_e}\langle b|e^{i\frac{\omega_{bg}-\omega}{c}\mathbf{n}\cdot\mathbf{r}}P_z G^{(+)}(E_g+\hbar\omega)e^{i\frac{\omega}{c}\mathbf{n}\cdot\mathbf{r}}P_z|g\rangle + \frac{1}{2}\langle b|e^{i\frac{\omega_{bg}}{c}\mathbf{n}\cdot\mathbf{r}}|g\rangle. \quad (16)$$

The integral in ω, denoted by $\mathcal{J}$ in the following, can be recast in the form

$$\mathcal{J} = \int_{\omega_{bg}/2}^{\infty} d\omega\varphi(\omega)\varphi(\omega_{bg}-\omega)[\mathcal{T}_{bg}(\omega)+\mathcal{T}_{bg}(\omega_{bg}-\omega)]. \tag{17}$$

But, using the explicit expression (16), we notice the relation

$$\mathcal{T}_{bg}(\omega)+\mathcal{T}_{bg}(\omega_{bg}-\omega) \equiv \mathcal{M}_{bg}^{\mathrm{KHW}}(\omega,\omega-\omega_{bg}), \tag{18}$$

with $\mathcal{M}_{bg}^{\mathrm{KHW}}$ being the KHW matrix element (3). Finally, we have

$$\mathcal{A}_{g\to b} = \frac{1}{2\pi i\hbar}\frac{(eA_0)^2}{m_e}\mathcal{J}, \tag{19}$$

with

$$\mathcal{J} = \int_{\omega_{bg}/2}^{\infty} d\omega\Phi(\omega_{bg},\omega)\mathcal{M}_{bg}^{\mathrm{KHW}}(\omega,\omega-\omega_{bg}), \tag{20}$$

where $\Phi(\omega_{bg},\omega)$ is the function (10). The probability of the transition induced by SRS is then

$$p_{g\to b} = |\mathcal{A}_{g\to b}|^2 = \frac{(eA_0)^4}{4\pi^2\hbar^2m_e^2}|\mathcal{J}|^2. \tag{21}$$

Equation (20) shows that, in the case of a pulse, we meet the KHW matrix element $\mathcal{M}_{bg}^{\mathrm{KHW}}(\omega,\omega')$ of stimulated Raman scattering in the presence of two *fictitious* monochromatic fields with frequencies ω and ω', satisfying the energy conservation law

$$E_g+\hbar\omega = E_b+\hbar\omega'. \tag{22}$$

The wave vectors of the two fields

$$\mathbf{k} = \frac{\omega}{c}\mathbf{n}, \quad \mathbf{k}' = \frac{\omega'}{c}\mathbf{n}, \tag{23}$$

are along the pulse direction $\mathbf{n}$, their difference being $\mathbf{k}-\mathbf{k}' = \omega_{bg}\mathbf{n}/c$. We note that the contribution to $\mathcal{J}$ due to absorption of two photons, coming for $\omega<\omega_{bg}$ (for which $\omega'<0$), is negligible for the photon energies corresponding to our pulse.

The numerical calculation of the matrix elements $\mathcal{M}_{bg}$ and of the integral $\mathcal{J}$ appearing in Eq. (20) is a rather difficult task, due to the presence of the Green operator and retardation factors. This is why we use the form given in Eq. (8) for the matrix element, with further approximations described below.

An efficient approximation of the amplitude (19) is obtained by taking into account the spectral properties of the pulse, manifested under the integral $\mathcal{J}$ by the overlap function (10). The Bohr frequency ω_{bg} and the pulse bandwidth $\Delta\omega$ are the two parameters which dictate the properties of Φ. If $\Delta\omega$ is comparable with ω_{bg} or higher, the overlap $\Phi(\omega_{bg},\omega)$ of the two Fourier transforms is significant. On the contrary, for $\Delta\omega$ less than ω_{bg} the function $\Phi(\omega_{bg},\omega)$ takes smaller values, going to zero in the case of the monochromatic field. Practically, the dominant contribution to the integral (20) comes from a frequency interval $\mathcal{I}$ slightly larger than $(\omega_0,\omega_0+\omega_{bg})$ (its width depends on the ratio $\Delta\omega/\omega_{bg}$); the function $\Phi(\omega_{bg},\omega)$ taking negligible values outside this interval. Approximating the matrix element $\mathcal{M}_{bg}(\omega,\omega-\omega_{bg})$ over this interval by its value at a frequency ω_1 between ω_0 and $\omega_0+\omega_{bg}$ (this being equivalent to neglecting the variation of the second-order coupling term, associated with $\mathbf{A}\cdot\mathbf{P}$), one obtains

$$\mathcal{J} \approx \mathcal{K}\mathcal{M}_{bg}^{\mathrm{KHW}}(\omega_1,\omega_2), \quad \text{with } \omega_2 \equiv \omega_1-\omega_{bg}, \tag{24}$$

with the notation

$$\mathcal{K} \equiv \int_{\mathcal{I}} d\omega\Phi(\omega_{bg},\omega) = \int_{\mathcal{I}} d\omega\varphi(\omega)\varphi(\omega_{bg}-\omega). \tag{25}$$

If we adopt the approximation described above, the final result for the transition amplitude is

$$\mathcal{A}_{g\to b} \approx \frac{1}{2\pi i\hbar}\frac{(eA_0)^2}{m_e}\mathcal{K}\mathcal{M}_{bg}^{\mathrm{KHW}}(\omega_1,\omega_2). \tag{26}$$

The corresponding transition probability is

$$p_{g\to b} = |\mathcal{A}_{g\to b}|^2 \approx \frac{(eA_0)^4|\mathcal{K}|^2}{4\pi^2\hbar^2m_e^2}\left|\mathcal{M}_{bg}^{\mathrm{KHW}}(\omega_1,\omega_2)\right|^2. \tag{27}$$

The spectral properties of the pulse, manifested only in the integral $\mathcal{K}$, are partially separated from those of the atom, the last ones entering in the matrix element $\mathcal{M}_{bg}^{\mathrm{KHW}}(\omega_1,\omega_2)$ and in $\mathcal{K}$ through the parameter ω_{bg}.

The optimal choice of ω_1 is in the middle of the interval in between ω_0 and $\omega_0+\omega_{bg}$. Thus we have

$$\omega_1 = \omega_0+\omega_{bg}/2, \quad \omega_2 = \omega_0-\omega_{bg}/2. \tag{28}$$

This choice leads to an improvement of the approximation (26) when the function $\Phi(\omega_{bg},\omega)$ is symmetric around ω_1, $\Phi(\omega_{bg},\omega_1-w) = \Phi(\omega_{bg},\omega_1+w)$. Indeed, in this case a *linear variation* (not necessary small) of $\mathcal{M}_{bg}^{\mathrm{KHW}}(\omega,\omega_{bg}-\omega)$ over the interval $\mathcal{I}$ (chosen symmetric around ω_1) can be ignored, since the integral $\int_{\mathcal{I}} d\omega\Phi(\omega_{bg},\omega)(\omega-\omega_1)$ vanishes. This situation arises in particular if the pulse has a shape described by an even function of time. Then, to a very good approximation, its Fourier transform $\varphi(\omega)$ is an even function of $\omega-\omega_0$ (for positive frequencies ω) and the product $\Phi(\omega_{bg},\omega)$ is symmetric around ω_1. We also note that ω_0 and $\omega_0+\omega_{bg}$ give the positions of the maxima of $|\varphi(\omega)|$ and $|\varphi(\omega-\omega_{bg})|$. This explains why usually their product, equal to $|\Phi(\omega_{bg},\omega)|$, has a pronounced maximum at ω_1 in the case $\Delta\omega>\omega_{bg}$.

In the numerical calculations we use the approximation (8) to calculate the matrix element $\mathcal{M}_{bg}^{\mathrm{KHW}}$. The formula (8), used in conjunction with Eq. (26) or (19), has the nice feature of leading, at the level of transition amplitudes or excitation probabilities, to the separation of the $\mathbf{A}\cdot\mathbf{P}$ and $\mathbf{A}^2$ contributions. This is easy to understand, taking into account that the corresponding selection rules are different: the first term in Eq. (8) is responsible for the Raman transitions to the *ns* and *nd* states, while the last term (related to retardation effects) leads to transitions to *np* states.

III. RESULTS AND DISCUSSION

We report calculations of SRS for a laser pulse with the peak intensity fixed at $I_0 = 3.51\times10^{16}$ W/cm^2 in a domain of the central frequency ω_0 ranging from 5 to 55 a.u.

Our numerical results are presented in Figs. 1 to 6. Data obtained with the TDSE are shown only in Fig. 1. In all other figures the results are provided by PT calculations; we did this because we have found a very good agreement between the output of these two approaches. We calculate the probability

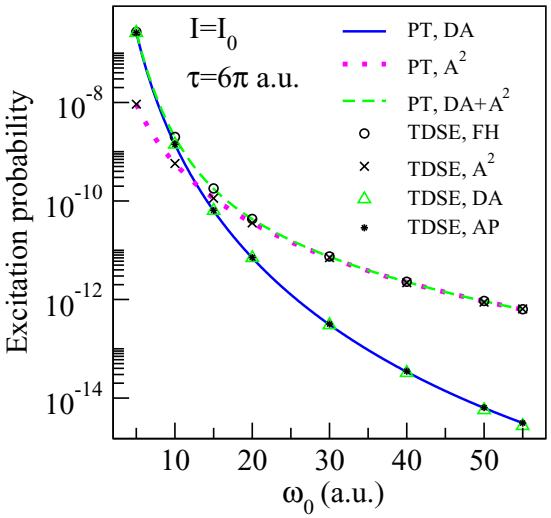

FIG. 1. Total excitation probability for a pulse with peak intensity $I = I_0$ and a total duration $\tau = 6\pi$ a.u. (≈0.48 fs). Comparison between results based on TDSE integration in different approximations (see text) and on perturbation theory (PT).

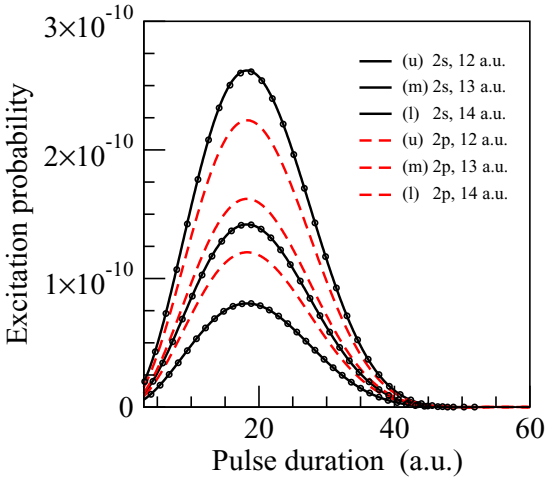

FIG. 2. Results in PT for the excitation probability of $2s$ (contribution of $\mathbf{A}\cdot\mathbf{P}$ in DA) and $2p$ states (contribution of $\mathbf{A}^2$), for a pulse with peak intensity $I = I_0$, and for several frequencies, indicated on the figure. The circle symbols show the approximate PT results for $2s$ states, calculated by using Eq. (27). The labels "u," "m," and "l" refer to upper, middle, and lower solid (dashed) lines, respectively.

of transition (21) in PT based on Eqs. (19) and (20), in which for the element matrix $\mathcal{M}$ we use the dipole approximation in the case of ns and nd transitions, with the analytic expressions given in the Appendix. The approximation (7) is used for the np transitions; the derivation of the analytic expression of the associated amplitudes is straightforward.

First, we refer to calculations performed for a pulse with a fixed duration $\tau = 6\pi$ a.u., whose the spectral width $\Delta\omega = 0.48$ a.u. is close to the ionization potential of the hydrogen atom. In Fig. 1 we present results based on TDSE integration and PT equations. The quantity represented is the total excitation probability, approximated by the sum over the $n = 2$–13 contributions, as a function of the pulse frequency $\omega_0 = 5$–55 a.u. The TDSE results are obtained: (i) in the dipole approximation (labeled "TDSE, DA" in the figure), (ii) including the first nondipole correction $\mathcal{H}^{(1)}_{\rm RET}$ beyond DA ("TDSE, AP"), (iii) keeping only the interaction term $\mathcal{H}^{(2)}_{\rm RET}$ originating from $\mathbf{A}^2$ term (label "TDSE, A^2"), and (iv) with the full Hamiltonian (13) ("TDSE, FH"). We also show in Fig. 1 perturbative results corresponding to cases (i) and (iii), indicated by the labels "PT, DA" and "PT, A^2," respectively, and their sum ("PT, DA + A^2").

We start the discussion by analyzing in Fig. 1 the results obtained with the TDSE. The comparison between TDSE-FH and TDSE-DA shows that retardation effects are important in the higher part of the frequency range, for $\omega_0 > 20$ a.u., and decrease progressively from high to low frequencies, becoming negligible for $\omega_0 < 10$ a.u. We extend the comparison in order to understand the relative role of the two nondipole corrections $\mathcal{H}^{(1)}_{\rm RET}$ and $\mathcal{H}^{(2)}_{\rm RET}$. Considering that, in Fig. 1, the "TDSE, AP" results are very close to those of "TDSE, DA" over the whole frequency interval, it is clear that the correction $\mathcal{H}^{(1)}_{\rm RET}$ plays a minor role. This clearly indicates that the retardation effect is mainly due to the term associated with $\mathbf{A}^2$, a feature directly confirmed by the "TDSE, A^2" calculation. We also note that the TDSE and LOPT results agree well (for the intensity and frequency range considered), both separately, for the DA and A^2 calculations, but also regarding their sum. The agreement between "TDSE, FH" and "PT, DA + A^2" results is expected since the selection rules in LOPT (given at the end of Sec. II C) lead to different final-l values for "PT, DA" and "PT, A^2," therefore the two contributions do not interfere.

In relation with Fig. 1, we have already noticed that the dominant contribution comes in the upper frequency range from the term $\mathbf{A}^2$, while in the lower-frequency part the contribution of $\mathbf{A}\cdot\mathbf{P}$ dominates. Figure 1 clearly indicates that the excitation mechanism changes within the interval 10–20 a.u., where a transitory regime is observed. To evaluate more precisely at what frequency this change occurs we compare in Fig. 2 the excitation probabilities for the states $2s$ (solid line) and $2p$ (dashed line), as a function of the pulse duration, calculated in perturbation theory for $\mathbf{A}\cdot\mathbf{P}$ (in DA) and considering only the nondipole term $\mathbf{A}^2$. The figure clearly shows that the relative role of the latter two contributions is inverted within the frequency interval 12–13 a.u. Decreasing the frequency, the relative importance of the $\mathbf{A}\cdot\mathbf{P}$ term increases rapidly. Figure 3, which differs from Fig. 2 by the photon frequencies considered, shows that, within the range $\omega_0 = 4$–6 a.u., the $\mathbf{A}\cdot\mathbf{P}$ (in DA) contribution overcomes the $\mathbf{A}^2$ one by more than one order of magnitude.

Figures 2 and 3 also illustrate the closing of the excitation channel at long pulse durations. The excitation probability increases first in the range of short durations, reaches a maximum, then goes to zero monotonically for long durations. Increasing the pulse duration, the laser bandwidth decreases and, for a duration of 50 a.u., the channel is practically closed. This is expected because, in this case, the laser bandwidth has a value $\Delta\omega \approx 0.18$ a.u., slightly less than a half of the Bohr frequency $\omega_{21} = 0.375$ a.u.

We now examine the pertinence of the approximation leading to Eq. (26). We recall that, within this approximation, we have assumed that the KHW matrix element in Eq. (20) varies

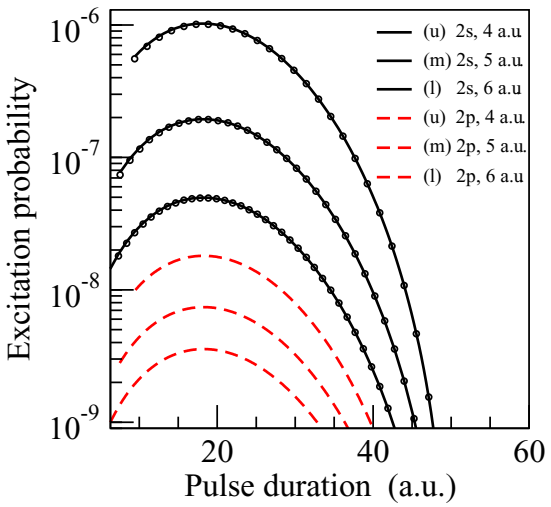

FIG. 3. Same as Fig. 2, except that the frequencies considered are 4, 5, and 6 a.u. For visibility, a logarithmic scale is used on vertical axis.

slowly with the frequency ω in the regions of interest. These considerations lead to a simple expression of the transition amplitude which finally involves a convolution product of pulse Fourier transforms calculated at two fixed frequencies. Calculations based on the approximate expression (26) are presented only in the case of $2s$ transitions (Figs. 2 and 3). In Figs. 2 and 3 we compare for the $2s$ state the PT results in DA, given by Eq. (21) (full lines), with the corresponding approximate PT results given by Eq. (27) (circles). The agreement observed confirms, for the actual conditions, the validity of the assumptions leading to Eq. (27).

In the next three figures (Figs. 4–6) we show results for a fixed frequency of 13 a.u., also considered in Fig. 2 for transitions to $2s$ and $2p$ states. Here we extend the presentation with the populations of ns, np, and nd states shown, respectively, in Figs. 4–6, as functions of the pulse duration. We also show the sum of the transition probabilities, for $n = 2$–5 and $n = 2$–13 in Figs. 4 and 5, and for $n = 3$–5 and $n = 3$–13 in Fig. 6.

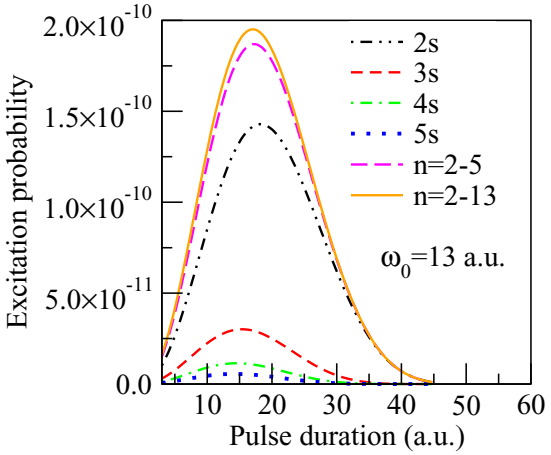

FIG. 4. PT results for excitation probabilities $1s \to ns$, with $n = 2$–5, and totals for $n = 2$–5 and $n = 2$–13. The peak intensity is I_0 and the frequency is fixed to 13 a.u.

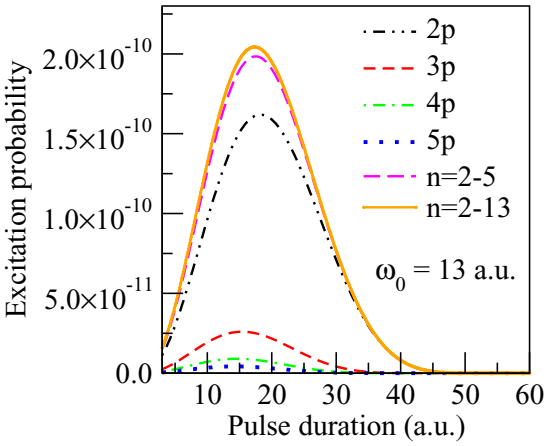

FIG. 5. The same as Fig. 4, now for np states.

Comparing Fig. 6 with Figs. 4 and 5, we note that the excitation probabilities of nd states are much smaller (by more than three orders of magnitude) than the excitation probabilities of ns and np states, a feature already observed in Ref. [17] at $\omega_0 = 55$ a.u. Here we also note that the excitation probabilities of ns and np states have comparable values.

In each of the above-mentioned figures we remark that the position of the maximum of the excitation probability shifts to a lower pulse duration with the increase of n. Also, the figures clearly show that the maximum value decreases rapidly with n; this is well illustrated in Figs. 4 and 5 by the quasiconvergence of the summation for $n = 2$–5. The similarity of Figs. 4–6 has a simple interpretation on the basis of the approximation (27). For a given pulse duration and quantum number n, the only change from one figure to another is the value of the matrix element $\mathcal{M}_{bg}$, which depends at most on ω_0 (and not on the other pulse parameters). As a consequence, the frequency ω_0 being the same in Figs. 4–6, the probabilities differ by a scaling factor on the vertical axis.

Finally, it is important to mention that we have checked that the results presented in Figs. 2–6 agree very well with TDSE calculations. This confirms the pertinence of the perturbation theory approach in our context. With the quadratic dependence of the probabilities with the intensity for SRS, one may predict much larger populations of bound states at higher intensities.

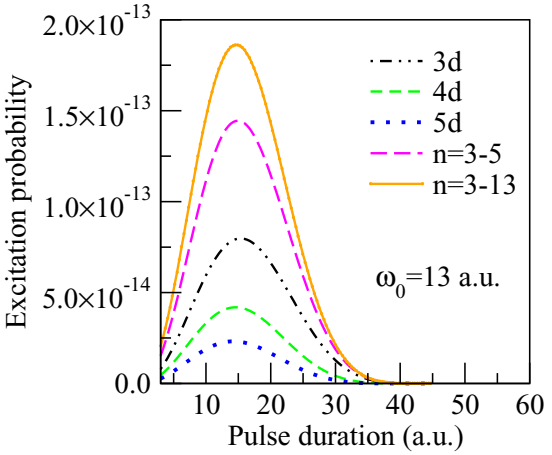

FIG. 6. Same as Fig. 4, but for nd states ($n \geqslant 3$).

Nevertheless, as noticed above, increasing the intensity, the perturbation theory might loose its validity. Also, relativistic effects of the order of $1/c^2$ or higher (in the atomic Hamiltonian or field-atom couplings), not considered in this paper, might become important. As recently demonstrated [23], at much higher peak intensities (beyond 10^{20} W/cm^2), for which the validity of PT becomes questionable, the retardation effects may change drastically the dynamics of excitation and ionization processes.

IV. CONCLUSIONS

We have investigated the excitation of the hydrogen atom in its ground state by stimulated Raman scattering of an ultrashort pulse with central frequencies ranging from 100 eV to 1.5 keV and a peak intensity of 3.51×10^{16} W/cm^2. The process occurs at sub-fs pulse durations (or fs durations, for the hydrogen atom initially in an excited state), for which the spectral bandwidth of the laser pulse is of the order of the Bohr frequencies of the atom. We used two approaches: a nonperturbative one, based on the numerical integration of the time-dependent Schrödinger equation, and a perturbative method. Both approaches include nondipole contributions of first order in $1/c$, originating from the interaction terms in the Hamiltonian. In the case of perturbation theory, we have developed the general formulation for the transition amplitude from which we have derived a simple approximate expression [see Eq. (26)]. The latter equation is the product of two contributions: the first factor is associated with the spectral properties of the pulse while the second term contains the atomic matrix elements; this simplifies considerably the calculations. There is a very good agreement between TDSE and PT calculations.

For the high-frequency range, from 55 a.u. down to around 20 a.u., the numerical results show that the contribution of the $\mathbf{A}^2$ term to the total excitation probability dominates by orders of magnitude that of the $\mathbf{A}\cdot\mathbf{P}$ term. Therefore, in the latter case, np states are preferentially populated, the population of ns states is much smaller but dominates that of the nd states. For the low-frequency domain, the roles of the interaction terms are reversed, the $\mathbf{A}\cdot\mathbf{P}$ (in DA) term dominating the effect for central frequencies of the order of a few a.u. The transitory regime is located in the range 10–15 a.u., where the probabilities are comparable. Below the latter frequency range the dipole approximation is valid and SRS mainly populates ns (and nd states to a lesser extent). It would be therefore of high interest to explore SRS around free-electron laser facilities, since these sources provide intense laser pulses in soft-x-ray regime with short pulse duration; the case of frequencies of few hundreds of eV is of particular interest in this context.

ACKNOWLEDGMENTS

This work has been supported by the COST Action CM1204 (Xlic) and by Project 29/2016 ELI RO financed by the Institute of Atomic Physics. The authors thank the University of Bordeaux for providing access to the Mésocentre de Calcul Intensif Aquitain (MCIA). This work was performed by using HPC resources from GENCI-IDRIS (Grant 2016-i2016057537).

APPENDIX: KRAMERS–HEISENBERG MATRIX ELEMENT FOR 1*s*-*ns* AND 1*s*-*nd* TWO-PHOTON TRANSITIONS

In the case of atomic hydrogen in the ground state, the matrix element (5) has a compact analytic expression for both ns and nd final states. In fact, analytic expressions for the two-photon bound-bound matrix element are available for any pair of bound states [24] and even with retardation included [25]. For the case we are interested in, according to Eq. (6) of Ref. [26],

$$\Pi_{33}^{(DA)}\big|_{ns,1s}(\Omega) = a(\tau) \text{ and } \Pi_{33}^{(DA)}\big|_{nd,1s}(\Omega) = \sqrt{5}b(\tau), \quad \text{(A1)}$$

with $\tau = 1/\sqrt{-2\Omega_{au}}$, $\mathrm{Re}\,\tau > 0$, and Ω_{au} the value of Ω taken in atomic units. The invariant amplitude $a(\tau)$ is a linear combination of three F_1 Appell functions of the variables

$$x_n = \frac{(1-\tau)(n-\tau)}{(1+\tau)(n+\tau)} \text{ and } y_n = \frac{(1-\tau)(n+\tau)}{(1+\tau)(n-\tau)}. \quad \text{(A2)}$$

The invariant amplitude $b(\tau)$ is a combination of two of these functions [see Eqs. (12)–(15) of Ref. [26]].

In the case $n = 1$ and $n = 2$ the amplitude $b(\tau)$ vanishes. The case $n = 1$ corresponds to Rayleigh scattering. In this case, by using the standard integral representation of the three Appell functions involved, the following simple result obtained,

$$a(\tau)|_{n=1} = \frac{2^7\tau^5}{(1+\tau)^8(2-\tau)}\,{}_2F_1(2-\tau,4,3-\tau;\,x_1) = \frac{1}{2}\frac{\tau}{2-\tau}\,{}_2F_1\left(1,4,3-\tau;\,\frac{x_1}{x_1-1}\right), \quad \text{(A3)}$$

coincides with the results of Gavrila given in Eqs. (54) and (55) of Ref. [27].

For $n = 2$ the result can be expressed simply as

$$a(\tau)|_{n=2} = \frac{2^{11/2}}{3^5}\left[\frac{3\tau}{2+\tau} - 2\frac{1-\tau}{3-\tau}\,{}_2F_1\left(1,5,4-\tau;\,\frac{x_2}{x_2-1}\right)\right], \quad \text{(A4)}$$

in agreement with Refs. [28,29].

For $n > 2$ each Appell function reduces to a sum of $(n-2)$ hypergeometric Gauss functions of the variable y_n. For $n = 3$ more compact expressions have been derived in Eqs. (29) and (30) of Ref. [30]. We have transformed them in order to eliminate

the apparent singularity they present at $\tau = 3$ and got

$$a(\tau)|_{n=3} = \frac{3\sqrt{3}}{64(2-\tau)(3+\tau)}\left(-9+24\tau-11\tau^2+5\frac{(1-\tau)^2(27-7\tau^2)}{(1+\tau)(3+\tau)(4-\tau)}\,{}_2F_1(1,\ -1-\tau, 5-\tau;\ x_3)\right),$$
$$b(\tau)|_{n=3} = \frac{3\sqrt{3}\tau^2}{8\sqrt{10}(2-\tau)(3+\tau)}\left(1+\frac{(1-\tau)^2}{(1+\tau)(3+\tau)(4-\tau)}\,{}_2F_1(1,\ -1-\tau, 5-\tau;\ x_3)\right). \quad \text{(A5)}$$

For large values of the principal number n the amplitudes $a(\tau)$ and $b(\tau)$ decrease as $n^{-3/2}$ [see Eqs. (21)–(23) of Ref. [26]].

[1] W. Ackermann *et al.*, Nat. Photonics **1**, 336 (2007).
[2] P. Emma *et al.*, Nat. Photonics **4**, 641 (2010).
[3] T. Ishikawa *et al.*, Nat. Photonics **6**, 540 (2012).
[4] G. Doumy *et al.*, Phys. Rev. Lett. **106**, 083002 (2011).
[5] H. Bachau, M. Dondera, and V. Florescu, Phys. Rev. Lett. **112**, 073001 (2014).
[6] M. Dondera, V. Florescu, and H. Bachau, Phys. Rev. A **90**, 033423 (2014).
[7] A. Marinelli *et al.*, Nat. Commun. **6**, 6369 (2015).
[8] H. Bachau, M. Dondera, and V. Florescu, J. Mod. Opt. **63**, 402 (2016).
[9] T. Tanaka, Phys. Rev. Lett. **110**, 084801 (2013).
[10] E. Prat and S. Reiche, Phys. Rev. Lett. **114**, 244801 (2015).
[11] E. Prat, F. Löhl, and S. Reiche, Phys. Rev. Spec. Top.–Accel. Beams **18**, 100701 (2015).
[12] E. Hemsing, G. Stupakov, D. Xiang, and A. Zholents, Rev. Mod. Phys. **86**, 897 (2014).
[13] Y. Ding, Proc. SPIE **9512**, 95121B (2015).
[14] S. Miyabe and P. Bucksbaum, Phys. Rev. Lett. **114**, 143005 (2015).
[15] G. Eckhardt, R. W. Hellwarth, F. J. McClung, S. E. Schwarz, D. Weiner, and E. J. Woodbury, Phys. Rev. Lett. **9**, 455 (1962).
[16] R. W. Hellwarth, Phys. Rev. **130**, 1850 (1963).
[17] H. Bachau and M. Dondera, Europhys. Lett. **114**, 23001 (2016).
[18] H. R. Reiss, Phys. Rev. Lett. **101**, 043002 (2008).
[19] M. Dondera and H. Bachau, Phys. Rev. A **85**, 013423 (2012).
[20] H. Bachau, O. Budriga, M. Dondera, and V. Florescu, Cent. Eur. J. Phys. **11**, 1091 (2013).
[21] H. A. Kramers and W. Heisenberg, Z. Phys. **31**, 681 (1925).
[22] I. Waller, Eur. Phys. J. A **51**, 213 (1928).
[23] A. S. Simonsen and M. Førre, Phys. Rev. A **93**, 063425 (2016).
[24] T. A. Marian, Phys. Rev. A **39**, 3816 (1989).
[25] T. A. Marian, Ph.D. thesis, University of Bucharest, 1990 (unpublished).
[26] V. Florescu, S. Patrascu, and O. Stoican, Phys. Rev. A **36**, 2155 (1987).
[27] M. Gavrila, Phys. Rev. **163**, 147 (1967).
[28] S. Klarsfeld, Lett. Nuovo Cimento Soc. Ital. Fis. **1**, 682 (1969).
[29] S. Klarsfeld, Phys. Rev. A **6**, 506 (1972).
[30] V. Florescu, Phys. Rev. A **30**, 2441 (1984).